Hydrogen-Bonding Structure of Serine Side Chains in *Bombyx mori* and *Samia cynthia ricini* Silk Fibroin Determined by Solid-State ^{2}H NMR

Tsunenori Kameda,[†] Yohei Ohkawa,[†] Keiko Yoshizawa,[†] Junko Naito,[†] Anne S. Ulrich,[‡] and Tetsuo Asakura*[,†]

Department of Biotechnology, Tokyo University of Agriculture and Technology, Koganei, Tokyo 184, Japan, and Institut für Molekularbiologie, Friedrich-Schiller-Universität Jena, Winzerlaer Strasse 10, 07745 Jena, Germany

Received April 12, 1999; Revised Manuscript Received June 16, 1999

ABSTRACT: Deuterium solid-state NMR was used to study the dynamics and molecular structure of the serine (Ser) side chains in silk fibroin from *Bombyx mori* and from *Samia cynthia ricini*. Samples were selectively labeled with [3,3-$^2H_2$]Ser, and the ^{2}H NMR powder spectra were analyzed by line shape simulation. Two types of motion could be characterized quantitatively: one component undergoing a rapid three-site jump (25%) and a second component representing a slow exchange between sites with unequal occupancies and with a small amplitude of libration (75%). From these results, it is concluded that approximately 75% of the Ser residues contribute to the formation of hydrogen bonds in both kinds of silk fibroin from *B. mori* and *S. cynthia ricini*. Furthermore, uniaxially oriented silk fibers were used to determine the side-chain conformation and the orientational distribution of the Ser residues in the slow motional component of *B. mori* silk fibroin. The *gauche*+ conformer around N−C_α−C_β−O was found to be dominant, suggesting that the hydroxyl groups of Ser interact with carbonyl groups on adjacent chains and thereby contribute to the intermolecular hydrogen-bonding network of the fiber.

Introduction

Silk fibroin from the domesticated silk worm *Bombyx mori* (*B. mori*) is a fibrous protein containing 46% glycine (Gly), 29% alanine (Ala), 12% serine (Ser), 4.8% tyrosine (Tyr), and 2.5% valine (Val).[1] The primary structure of *B. mori* silk fibroin has been determined by Mita et al.,[2] who showed that the sequence consists of repetitive (Gly−Ala−Gly−Ala−Gly−Ser−)$_n$ and nonrepetitive regions. Interestingly, the wild silkworm *Samia cynthia ricini* (*S. cynthia ricini*) has an amino acid composition and sequence rather different from *B. mori*. The primary structure of the silk fibroin from *S. cynthia ricini* has recently been determined by Yukuhiro et al.,[3] which was very similar to the structure of silk fibroin from *Antheraea pernyi*.[4] This kind of silk fibroin is largely made up of repetitive regions, each consisting of a polyalanine stretch of 10−14 residues that is followed by a Gly-rich sequence. Its total amino acid composition contains 33.2% Gly, 48.4% Ala, 5.5% Ser, 4.5% Tyr, and 0.4% Val. In both kinds of silk, the relatively abundant Ser residue is of particular interest, as it carries a hydroxyl group that may engage in hydrogen bonding and thus contribute to the stability of the fiber. Therefore, it is important to clarify the structure and dynamics of the Ser side chain. In *B. mori* fibroin, about 75% of all Ser residues occur within the sequence of the repetitive region,[2] which is considered to be the crystalline domain of fibroin.[5] In contrast, in *S. cynthia ricini*, virtually all of the Ser residues are found in the Gly-rich region of the sequence, which might be expected to have less tendency to assume any defined secondary structure. Early X-ray diffraction studies had proposed that *B. mori* silk fibroin in the fibrous state forms an antiparallel β sheet, on the basis of models of a repetitive sequence of −(Gly−Ala)$_n$.[1,6,7] Later, the local backbone torsion angles (ϕ, ψ) of the Ala and Gly residues were determined from angular constraints obtained by solid-state NMR studies on ^{15}N- and ^{13}C-labeled fibers.[8−10] More recently, Asakura et al. have shown that the Ser, Tyr, and Val residues of *B. mori* silk fibroin also occupy a restricted conformational space in the antiparallel β sheet region.[11] By means of ^{13}C NMR, they have furthermore characterized the secondary structure of silk fibroin from *S. cynthia ricini* and were able to demonstrate unambiguously that also in this kind of unrelated sequence the Ala residues are present as antiparallel β sheets.[12]

^{2}H NMR spectroscopy is a powerful approach to examine the molecular motion of polymers in the solid state.[13−15] Different types of motion can be discriminated on the basis of their time scale and their geometry of exchange. The one-dimensional quadrupole echo line shape of ^{2}H NMR is especially sensitive to dynamics in the range of 10^{-8} s < τ_c < 10^{-3} s, where τ_c is the motional correlation time.[16] Within these limits, the ^{2}H NMR line shape can comprehensively be analyzed in terms of well-known models to yield the geometry and rate of segmental motion. Solid-state ^{2}H NMR thus offers the possibility of examining the dynamics of the Ser side chain and thereby observing the formation of hydrogen bonds via the hydroxyl group. Hydrogen bonding is expected to lead to a restriction in motion by decreasing the rotational freedom of the three-site jump about the C_α−C_β axis. In a previous ^{2}H NMR study of *B. mori* silk fibroin, the reorientation of most Ser side chains was reported virtually to be frozen.[17] This observation suggested that the hydroxyl group of Ser may contribute to intra- or interchain hydrogen bonds. The spin−lattice relaxation time of the C_β carbon on Ser was observed to consist of two components, which were attributed to hydroxymethyl groups participating in hydrogen bonds

[†] Tokyo University of Agriculture and Technology.
[‡] Friedrich-Schiller-Universität Jena.

10.1021/ma990554q CCC: $18.00
Published on Web 09/15/1999

and to those that are not involved in any.[18] However, there is little quantitative information about the structural aspects of the postulated Ser side-chain hydrogen bonds, which would be required to draw a correlation between the protein secondary structure and the stability of the fiber.

When an oriented sample is available for ^{2}H NMR, such as a drawn fiber, it is possible to measure directly the orientation of the labeled C$-^2$H bond vector with respect to the sample axis and thereby to determine the local three-dimensional molecular structure.[19] For example, Lee and Cross have studied the structure and dynamics of ^{2}H-labeled Val side chains on gramicidin A in oriented lipid bilayers.[20] In a recent study on oriented silk fibers, we have measured the angle between the fiber axis and the side-chain bond vectors of [2,2-$^2H_2$]Gly and [3,3,3-$^2H_3$]Ala in *B. mori*.[21,22] The atomic coordinates and backbone torsion angles (ϕ, ψ) of Gly and Ala were accurately determined from these angles and other structural constraints derived by solid-state NMR.

In the present study, we have characterized and compared the Ser side-chain dynamics of *B. mori* and *S. cynthia ricini* silk fibroin by solid-state ^{2}H NMR. A detailed line shape analysis has provided quantitative data on the rate of motion and on the fractions of two distinct dynamic populations. In addition, the torsion angle of the Ser C$_\alpha-$C$_\beta$ bond and its orientational distribution were measured in uniformly aligned silk fibers.

Materials and Methods

Materials. Selective isotope labeling of *B. mori* and *S. cynthia ricini* silk fibroin is necessary for these NMR experiments to obtain site-specific structural information. Labeling was achieved biosynthetically by feeding silk worms during the fifth instar larval stage with an artificial diet supplemented with the isotope-labeled amino acid [3,3-$^2H_2$]Ser.[23] The isotope-labeled silk fibroin from *B. mori* was collected from the cocoons and used for NMR after removing another silk protein, sericin.[24] The isotope-labeled silk fibroin from *S. cynthia ricini* was collected from either the cocoons or the silk glands for the preparation of nonoriented and oriented samples, respectively. The liquid silk stored in the silk glands was drawn at a constant speed of 1.6 m min^{-1} to produce fibers, and the tissue of the silk gland was removed. The reason we used silk fibroin from the silk gland instead of the cocoons is that it is difficult to prepare oriented fibers (see below) from the cocoons of *S. cynthia ricini*. Our previous comparison of ^{15}N NMR spectra of oriented silk fibroin from *Bombyx mori* cocoons and silk glands had shown that the spectra were essentially the same. Hence, the different ways of sample preparation (from cocoons or silk glands) do not affect the structure or the degree of orientation.[25] To prepare oriented NMR samples, thin sheets of uniformly aligned fibers were fixed with a quick-setting glue and cut into 4 × 10 mm pieces. These sheets were then glued together as a 4 × 10 × 6 mm stack that fits into the 10 mm diameter of the radio frequency NMR coil.[26]

^{2}H NMR Experiments and Theoretical Calculations. To determine the labeling ratio, solution-state ^{2}H NMR spectra were acquired of 3.0% (w/w) ^{2}H-labeled silk fibroin in TFA, using an EX 400 NMR spectrometer. Solid-state NMR spectra were recorded at 61.06 MHz on a Chemagnetics cmx Infinity 400 spectrometer equipped with a solid-state ^{2}H NMR unit. The quadrupole echo pulse sequence (90°$x - \tau_1 -$ 90°$y - \tau_2 -$ echo, where τ_1 and τ_2 are delay times) was used with a 90° pulse length of 3.2 μs. Because the echo maximum is not observed exactly at $\tau_1 = \tau_2$ due to finite pulse widths,[16] appropriate leftshifts were applied to give effective intervals of $\tau_1 = 50$ and $\tau_2 = 55$ μs. The spectral width was 2000 kHz, 8192 data points were collected, and the number of scans was 6000−20 000. The repetition time was 10 s for silk fibroin and 20 s for the crystalline amino acid. Lorentzian line broadening of 4 kHz was applied, and spectra were symmetrized to improve signal-to-noise. Spectra were acquired at room temperature, unless noted otherwise.

Line Shape Analysis. Quadrupole echo ^{2}H NMR powder spectra were simulated using the program MXQET,[27] as a function of the exchange rate and libration angle, according to an appropriate dynamic model. For oriented samples, the line shape simulation is more complex and deserves further explanation. The electric field gradient tensor of a deuterium substituent is virtually axially symmetric and aligned along the C$-^2$H bond axis. Therefore, the angle θ of this C$-^2$H bond vector with respect to the magnetic field can be determined directly from the spectral quadrupole splitting $\Delta\nu_Q$, according to[28−30]

$$\Delta\nu_Q = \frac{3}{4}Q_{cc}(3\cos^2\theta - 1) \tag{1}$$

where Q_{cc} is the rigid lattice quadrupole coupling constant and the asymmetry parameter (η) is assumed to be zero. In the simplest case of a single crystal, where all labeled C$-^2$H bonds are aligned in the same direction with respect to the magnetic field, the resulting spectrum will consist of a pair of narrow lines. Similarly, in the case of a fiber that is oriented parallel to the spectrometer field, all C$-^2$H bond vectors lie along the rim of a cone around the fiber axis with an angle γ that is equivalent to θ. It is thus possible to determine the C$-^2$H bond angle relative to the fiber axis directly from the measured quadrupole splitting $\Delta\nu_Q$, using eq 1.

On the other hand, in a powdered sample or in an amorphous region of a fiber, all angles of θ between 0° and 180° contribute to the spectrum.[19] The intensity envelope of the resulting powder line shape is then calculated as the spherically weighted sum over all orientations of θ in space:[19]

$$P(\theta) = \frac{1}{2}(\sin\theta) \tag{2}$$

Between the two extremes of a single-crystal spectrum on one side and a powder line shape on the other, lies the situation of a fiber that is tilted with respect to the external magnetic field. In this case, the uniaxially oriented C$-^2$H bond vectors assume a certain range of values for θ that contribute to the spectrum. The resulting line shape is calculated as a function of the reduced resonance frequency $\zeta_\pm = \pm(3\cos^2\theta - 1)/2$, according to[31,32]

$$P_\pm = \frac{1}{\sqrt{\frac{\pm 2\zeta_\pm + 1}{3}}\sqrt{\sqrt{\frac{\pm 2\zeta_\pm + 1}{3}} - \cos(\alpha + \gamma)}\sqrt{\cos(|\alpha - \gamma|) - \sqrt{\frac{\pm 2\zeta_\pm + 1}{3}}}} \tag{3}$$

Here, γ represents the angle of interest between the C$-^2$H bond vector and the fiber axis, and the sample tilt angle α is manually adjusted between the fiber axis and the external magnetic field. This kind of line shape can possess up to three pairs of singularities, whose positions depend on the value of γ and vary with the sample inclination α.[19] The analysis of tilted samples is essential in situations where the value of θ cannot be calculated uniquely from the quadrupole splitting at $\alpha = 0°$ due to an indeterminate sign of $\Delta\nu_Q$. More generally, a line shape analysis of tilted samples ($\alpha \neq 0°$) provides a sensitive tool to verify or discard molecular models about an expected orientational distribution or motional averaging. In this study, we analyzed the line shapes for two orientations of the silk fibers, namely, parallel and perpendicular to the magnetic field. To account for the spectral line widths, a Gaussian distribution (eq 4) was assumed for the angle γ[33] as well as for the N$-$C$_\alpha-$C$_\beta-$O torsion angle (χ) of the Ser side chain, and an additional Gaussian line broadening was applied

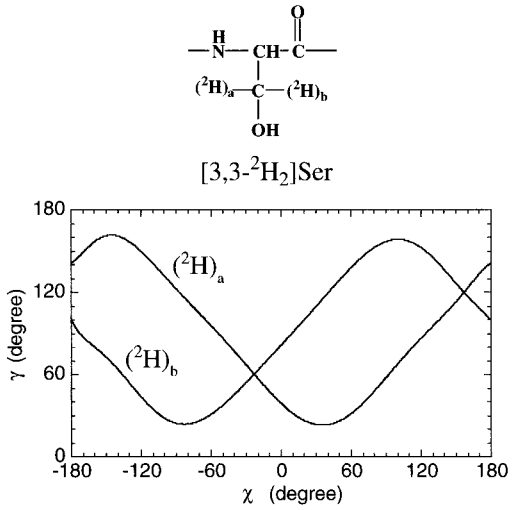

Figure 1. Angle γ between the $C_\beta-^2H$ bond vector and the fiber axis calculated as a function of the torsion angle χ around the $N-C_\alpha-C_\beta-O$ axis, based on a uniaxially oriented β sheet protein structure.

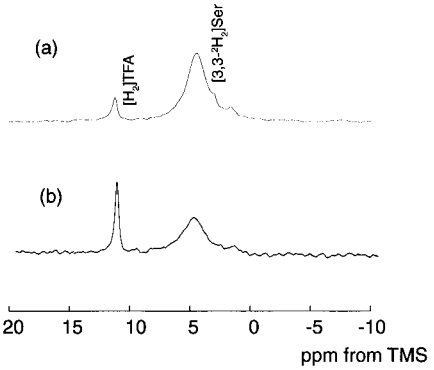

Figure 2. Solution-state ^2H NMR spectra of [3,3-$^2H_2$]Ser-labeled *B. mori* (a) and *S. cynthia ricini* (b) silk fibroin, dissolved in trifluoroacetic acid. These samples were obtained from cocoons after rearing the silk worm.

to the simulated spectra.

$$P(\phi) = N \exp\left(-\frac{\sin^2 \phi}{2 \sin^2 \bar{\phi}}\right) \quad \phi = \gamma \text{ or } \chi \tag{4}$$

In a uniaxially oriented silk fiber with a β sheet conformation, the $C_\alpha(i-1) - C_\alpha(i+1)$ direction is aligned parallel to the sample axis. Using this assumption and standard peptide bond lengths and angles,[34] the relationship between χ and γ is illustrated in Figure 1.

In this figure, the angle γ was calculated by rotating the torsion angle χ for the $C_\alpha-C_\beta$ axis over 360° in 0.5° increments. The two lines in the graph correspond to the two $C_\beta-^2H$ substituents on Ser, which differ only in terms of a phase shift along χ. When the fiber axis is aligned parallel ($\alpha = 0°$), θ is equal to γ and can be determined directly from the observed quadrupole splitting. Using the correlation of Figure 1, the expected line shape of the tilted sample ($\alpha = 90°$) is then calculated according to eqs 3 and 4 as a function of the angle χ. The simulated spectra are used to fit and confirm the experimental data.

Results and Discussion

1. Determination of the Isotope-Labeling Ratio. Figure 2 shows the solution-state ^2H NMR spectrum of [3,3-^{2} H_2]Ser-labeled silk fibroin dissolved in TFA.

The natural-abundance COO^2H peak of TFA served as a chemical shift reference (11.3 ppm from TMS[35]),

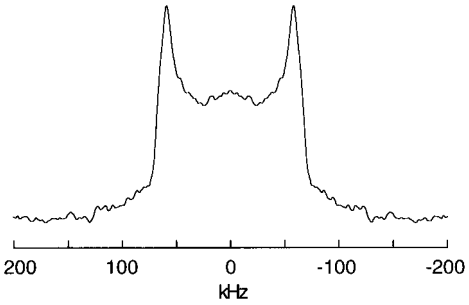

Figure 3. ^2H NMR quadrupole echo spectrum of the crystalline amino acid [3,3-$^2H_2$]*D,L*-Ser.

and its intensity was used to estimate the degree of ^2H incorporation. There is essentially no natural-abundance ^2H background from silk fibroin under the experimental conditions used. In the spectra of Figure 2, only one sharp peak at around 5 ppm is observed besides the TFA signal, and it is assigned to the incorporated [3,3-$^2H_2$]Ser. Any metabolic pathways from Ser to other amino acids thus appear to be negligible. The labeling ratio is high enough for both silk fibroin samples from *B. mori* and *S. cynthia ricini* to be suitable for solid-state NMR.

2. ^2H Solid-State NMR of Crystalline [3,3-$^2H_2$]DL-Ser. Figure 3 shows the ^2H NMR spectrum of the pure amino acid [3,3-$^2H_2$]DL-Ser as a powdered sample.

From X-ray diffraction analysis,[36-38] it was reported that all hydroxyl groups in the crystal are engaged in three hydrogen bonds, namely, a hydrogen bond to two carboxyl groups and to one nitrogen atom in the $-NH3+$ group. Because the three-site jump about the $C_\alpha-C_\beta$ bond is essentially frozen in the crystalline state, we consider this powder pattern as a reference for the rigid lattice at room temperature. The observed splitting of 173 kHz corresponds to $Q_{cc} = 157$ kHz and will be used in the simulations of silk fibroin. The powder line shape is indeed axially symmetric ($\eta = 0$).

3. ^2H Solid-State NMR of [3,3-$^2H_2$]Ser-Labeled *B. mori* and *S. cynthia ricini* Silk Fibroin. Figure 4a,bshows the ^2H NMR spectra of [3,3-$^2H_2$]Ser-labeled silk fibroin from *B. mori* and *S. cynthia ricini*.

The powder patterns (parts a and b) of the nonoriented silk fibers display no appreciable difference between *B. mori* and *S. cynthia ricini*. Both proteins give rise to the same set of quadrupole splittings of about 35.5 and 109.3 kHz. The inner component with a splitting of 35.5 kHz stems from Ser side chains undergoing rapid rotational motion, whereas the outer splitting represents comparatively immobile residues. A small central peak at zero frequency must be attributed to residual ^2HHO in the sample.[39] The line shapes of Figure 4c,d were simulated using the MXQET program developed by Greenfield et al.,[27] where the exchange rate and libration angle are calculated on the basis of appropriate dynamic models. The experimental spectra could properly be fitted as a sum of three components, namely, the two types of motionally distinct Ser side chains, plus a small ^2HHO contribution with a Gaussian line shape. The best-fit parameters of these simulations are summarized in Table 1.

As shown in Figure 4c, the spectrum for *B. mori* could be well-simulated assuming that the slow motional component contributes 75% and the rigid component 25% of the total intensity (see Table 1). The slow motional component in Figure 4c was simulated assuming a discrete three-site jump of the Ser side chain, with

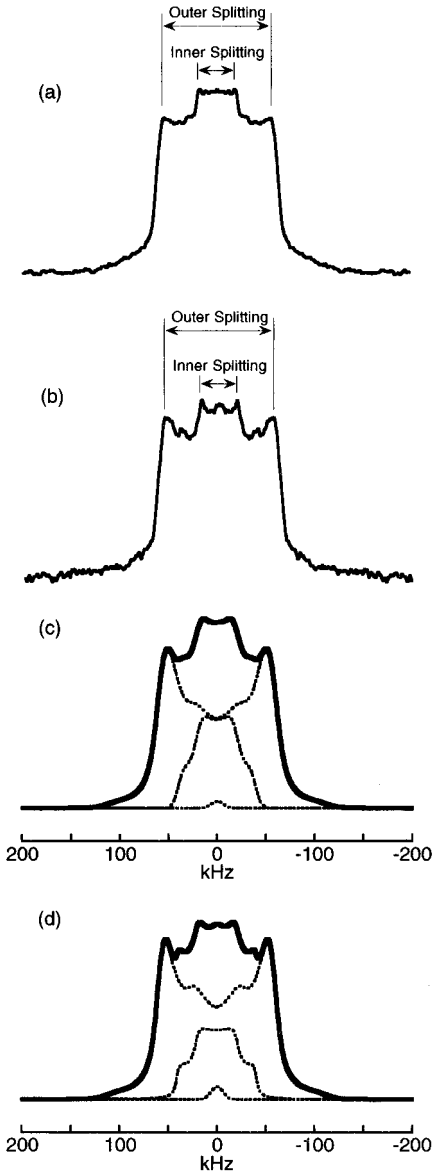

Figure 4. Experimental ^{2}H NMR powder spectra obtained from [3,3-$^2H_2$]Ser-labeled *B. mori* (a) and *S. cynthia ricini* (b) silk fibroin. The respective line shapes (c) and (d) were simulated on the basis of a three-site jump model, showing one fast and one slow motional component each, plus a small contribution of ^{2}HHO.

Table 1. Powder Pattern Line Shape Simulation Results of ^{2}H Quadrupole Experiments for [3,3-$^2H_2$]Ser-Labeled *B. mori* and *S. cynthia ricini*

component	rate (Hz)	occupancy	libration (deg)	fraction(%)
		B. mori		
fast	1×10^6	(33:33:33)	0	25
slow	5×10^3	(90:5:5)	15	75
		S. cynthia. rincini		
fast	1×10^6	(33:33:33)	0	22
slow	5×10^3	(80:10:10)	15	78

unequal occupancies (90:5:5 ratio) and a small librational amplitude. The fast component of *B. mori* satisfies a rapid three-site jump with equal occupancies. Likewise, the spectrum for *S. cynthia ricini* in Figure 4d could be simulated with 78% corresponding to a slow three-site jump with unequal occupancies (80:10:10 ratio) and a small librational amplitude, whereas the remaining 22% arise from a rapid three-site jump. Interestingly, these results indicate that there are no significant differences in the respective dynamic populations of *B. mori* and *S. cynthia ricini* silk fibroins, despite their unrelated amino acid sequences.

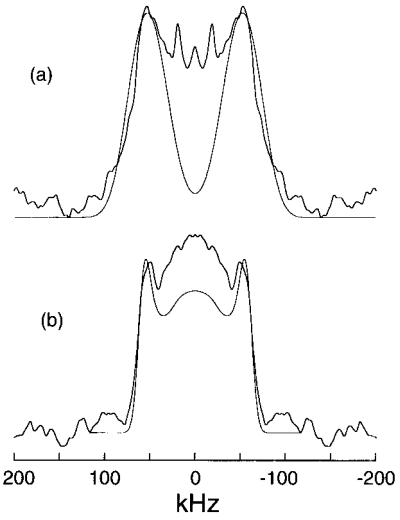

Figure 5. ^{2}H NMR quadrupole echo spectra of uniaxially aligned [3,3-$^2H_2$]Ser-labeled silk fibroin of *B. mori*. The fiber axis was set parallel (a) and perpendicular (b) to the magnetic field direction.

The motional freedom of the Ser side chain is expected to be constrained severely by hydrogen bonding between the hydroxyl group and adjacent backbone atoms. Therefore, the component with the rapid three-site jump is interpreted to arise from Ser residues that do not form hydrogen bonds. The groups involved in inter- or intrachain hydrogen bonding, on the other hand, are attributed to the slow motional component. On the basis of these assumptions, it is apparent that about $^3/_4$ of all Ser side chains form hydrogen bonds in both *B. mori* and *S. cynthia ricini*, with this fraction being almost the same despite the difference in molecular structure. We note that intermolecular hydrogen bonding between Ser and carbonyl groups on adjacent protein chains can occur irrespective of the primary and secondary structure, because the hydroxyl group is rather flexible. Therefore, the similar ratio of hydrogen-bonded compared to free hydroxyl groups in *B. mori* and *S. cynthia ricini* is consistent with a similar interchain environment around serine, despite its different abundance and distribution in the amino acid sequences.

Next, to examine the hydrogen-bonded structure of the Ser side chain, we investigated in more detail the conformation of those residues with low mobility. As the side chain is being rotated about its N$-$C$_\alpha-$C$_\beta-$O bond, the hydrogen bond length will vary. The limiting distance for hydrogen bonding is approximately 2.6$-$3.4 Å.[40] Another factor that has to be taken into account concerns the energetic preference for staggered conformations. The trans (t) and the two gauche ($g-$ and $g+$) side-chain conformations are strongly favored relative to any eclipsed conformation.[41] As described above, the powder pattern analysis of the slow motional component had indicated that the Ser side chain undergoes a three-site jump, with one dominant conformer existing among these sites. The torsion angle χ of this preferred conformer can be determined from the quadrupole splitting of uniformly aligned silk fibers. Figure 5 shows the ^{2}H NMR spectra of uniaxially aligned [3,3-$^2H_2$]Ser-labeled *B. mori* silk fibroin, with the fiber axis set parallel ($\alpha = 0°$) and perpendicular ($\alpha = 90°$) to the magnetic field direction, respectively.

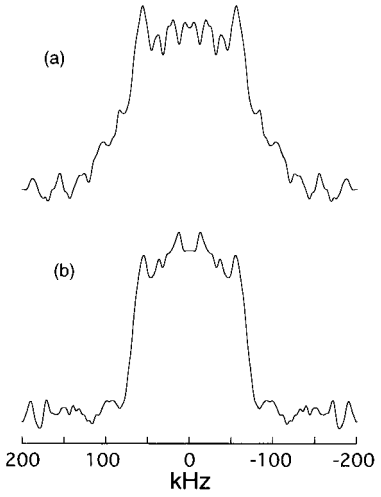

Figure 6. Experimental and calculated ^{2}H NMR spectra of uniaxially aligned [3,3-$^2H_2$]Ser-labeled *B. mori* silk fibroin at low temperature (−50 °C), where the fiber axis was set parallel (a) and perpendicular (b) to the magnetic field direction.

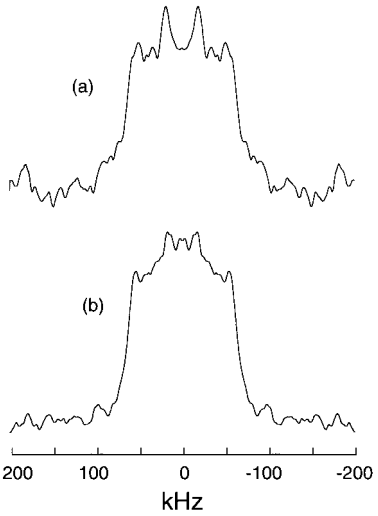

Figure 7. ^{2}H NMR quadrupole echo spectra of uniaxially aligned [3,3-$^2H_2$]Ser-labeled silk fibroin of *S. cynthia ricini*, where the fiber axis was set parallel (a) and perpendicular (b) to the magnetic field direction.

The line shapes show an appreciable dependence on the angle α, which indicates that Ser side chains are indeed reasonably well oriented with respect to the fiber axis. The inner and outer peak doublets observed in Figure 5a are consistent with splittings of 37.4 and 109.7 kHz, respectively, although the signal-to-noise ratio is rather low. The inner splitting must be attributed to the side chains undergoing the rapid three-site jump about the $C_\alpha-C_\beta$ axis, because of the relatively sharp line width. To confirm these assumptions, we carried out a low-temperature measurement with the uniaxially oriented sample of *B. mori* at −50 °C (Figure 6). The ^{2}H NMR spectra of Figure 6 show a pronounced orientation dependence, for both the inner singularities with a well-resolved splitting of 37.4 kHz and the outer component with a 109.7 kHz splitting. The intensity of the inner component has decreased with decreasing temperature, as expected from our assumption that it arises from the rapid three-site jump about the $C_\alpha-C_\beta$ axis. Therefore, the outer splitting of 109.7 kHz is attributed to the Ser side chains exhibiting slow motion.

The outer peaks in Figure 5a are significantly broadened, which indicates the superposition of a number of subspectra. These multiple contributions reflect not only the orientational distribution, but they must also be due to the existence of three staggered conformations about the $N-C_\alpha-C_\beta-O$ segment. However, in view of the pronounced preference for only one particular conformation, it is justified to approximate the line shape simulation by a single torsion angle (χ). According to the relationship described in Figure 1, each value of χ gives rise to two quadrupole splittings which represent the two $C_\beta-{}^2H$ substituents. We determined the best-fit value of χ by simulating the line shapes for the corresponding values of γ, including some line broadening due to the spread of orientations. The experimental data in parts a (α = 0°) and b (α = 90°) of Figure 5 can adequately be fitted assuming a Gaussian distribution for both angles χ and γ, with a width of $\bar{\chi} = \bar{\gamma} = 5°$. The important result of these simulations is the value of the preferred torsion angle χ = 67°, which corresponds to the two intramolecular ^{2}H bond angles of γ = 36° and 144°. The calculated spectrum accounts for about 75% of the total intensity, and this fraction agrees well with the expected population of the slow-motional component for *S. cynthia ricini* silk fibroin, as shown in Table 1. Given the value of χ = 67°, we conclude that the dominant conformer of the Ser side chain of *B. mori* silk fibroin exists in the *g*+ conformation. This *g*+ conformation is a good candidate for forming intermolecular hydrogen bonds with carbonyl groups on adjacent protein chains. In support of this result, Takahashi had also predicted a *g*+ conformation for the Ser side chain of *B. mori* from X-ray diffraction analysis.[7]

Finally, we carried out a similar analysis with [3,3-$^2H_2$]Ser-labeled *S. cynthia ricini* silk fibroin. Figure 7a,b shows the ^{2}H quadrupole echo spectra of the uniaxially aligned sample with the fiber axis set parallel (α = 0°) and perpendicular (α = 90°) to the magnetic field direction, respectively.

In this case, no significant difference is observed between the line shapes at the two different sample orientations. Moreover, these spectra are quite similar to the powder pattern shown in Figure 4b. These results indicate that in *S. cynthia ricini* the Ser side chains are not that uniformly oriented with respect to the fiber axis. More recently, we have quantitatively analyzed and compared the orientational distribution of Ala and Gly residues in silk fibers from both *B. mori*[42] and *S. cynthia ricini* by solid-state NMR.[12] We found that more than 60% of all Gly residues are oriented for both *B. mori* and *S. cynthia ricini*. However, the degree of orientation is rather different between the two kinds of silk, as the Gly-rich region of *S. cynthia ricini* possesses a significantly wider distribution of orientations than that of the repetitive region of *B. mori* silk fibroin. This finding is consistent with our present observation that the orientational distribution of the Ser side chains, too, is wider in *S. cynthia ricini* than that in *B. mori*.

Conclusions

The dynamics and local structures of the Ser side chains in *B. mori* and *S. cynthia ricini* silk fibroins have been characterized by ^{2}H solid-state NMR. Not only the powder spectra but also the line shapes from uniaxially oriented samples have been analyzed for [3,3-$^2H_2$]Ser-labeled fibroin by computer simulation. We found that approximately 75% of the Ser side chains form hydrogen bonds, and the remaining 25% are not involved in any.

The hydrogen-bonded component in *B. mori* was shown to undergo a slow three-site jump, in which the occupancy of the sites corresponds to the ratio 90:5:5. By measuring the dominant side-chain torsion angle of the $N-C_\alpha-C_\beta-O$ axis, we concluded that the preferred structure corresponds to a *gauche*+ conformation. This result suggests that Ser forms interchain hydrogen bonds.

Acknowledgment. T.A. acknowledges supports of the Grant-in-Aid for JSPS Fellows and the Program for Promotion of Basic Research Activities for Innovative Biosciences, Japan. A.S.U. acknowledges the DFG for TP B13 in SFB 197.

References and Notes

(1) Asakura, T.; Kaplan, D. L. In *Encyclopedia of Agricultural Science*; C. J., Arutzen, Ed.; Academic Press: London, 1994; Vol. 4, pp 1−11.
(2) Mita, K.; Ichimura, S.; James, T. C. *J. Mol. Evol*. **1994**, *38*, 583.
(3) Yukuhiro, Y.; Kanda, T.; Tamura, T., personal communication.
(4) Yukuhiro, Y.; Kanda, T.; Tamura, T. *Insect Mol. Biol*. **1997**, *6*, 89.
(5) Strydom, D. J.; Haylett, T.; Stead, R. T. *Biochem. Biophys. Res. Commun*. **1977**, *79*, 932.
(6) Marsh, R. E.; Corey, R. B.; Pauling, L. *Biochim. Biophys. Acta* **1955**, *16*, 1.
(7) Takahashi, Y.; Gehoh, M.; Yuzuriha, K. *J. Polym. Sci., Part B.; Polym. Phys*. **1991**, *29*, 889.
(8) Asakura, T.; Kuzuhara, A.; Tabata, R.; Saito, H. *Macromolecules* **1985**, *18*, 1841.
(9) Asakura, T.; Demura, M.; Date, T.; Miyashita, N.; Ogawa, K.; Williamson, M. P. *Biopolymers* **1997**, *41*, 193.
(10) Asakura, T.; Demura, M.; Nishikawa, N.; Yoshimizu, H. In *Solid State NMR of Polymers*; Ando, I.; Asakura, T., Eds.; Elsevier: New York, 1998; pp 853−890.
(11) Asakura, T. et al., to be submitted for publication.
(12) Asakura, T.; Ito, T.; Okudaira, M.; Kameda, T. *Macromolecules* **1999**, *32*, 4940.
(13) Davis; J. K.; Jeffrey, K. R.; Bloom, M.; Valic, M. I.; Higgs, T. P. *Chem. Phys. Lett*. **1976**, *42*, 390.
(14) Spiess, H. W. *Colloid Polym. Sci*. **1983**, *261*, 193.
(15) Torchia, D. A. *Annu. Rev. Biophys. Bioeng*. **1978**, *13*, 125.
(16) *Nuclear Magnetic Resonance Probes of Molecular Dynamics*; Tycko, R., Ed.; Kluwer Academic Publishers: Boston, 1994; pp 27−106.
(17) Saito, H.; Tabeta, R.; Kuzuhara, A.; Asakura, T. *Bull. Chem. Soc. Jpn*. **1989**, *59*, 3383.
(18) Saito, H.; Ishida, M.; Yokoi, M.; Asakura, T. *Macromolecules* **1990**, *23*, 83.
(19) Ulrich, A. S.; Grage, S. L. In *Solid State NMR of Polymers*; Ando, I., Asakura, T., Eds.; Elsevier: New York, 1998; pp 190−211.
(20) Lee, K.-C.; Cross, T. A. *Biophys. J*. **1994**, *66*, 1380.
(21) Asakura, T.; Minami, M.; Shimada, R.; Demura, M.; Osanai, M.; Fujito, T.; Imanari, M.; Ulrich, A. S. *Macromolecules* **1997**, *30*, 2429.
(22) Asakura, T.; Demura, M.; Nishikawa, N. *Annu. Rep. NMR Spectrosc*. **1997**, *34*, 302.
(23) Asakura, T.; Sakaguchi, R.; Demura, M.; Ogawa, K.; Osanai, M. *Biotechnol. Bioeng*. **1993**, *41*, 245.
(24) Nicholson, L. K.; Asakura, T.; Demura, M.; Cross, T. A. *Biopolymers* **1993**, *33*, 847.
(25) Asakura, T.; Yeo, J. H.; Demura, M.; Itoh, T.; Fujito, T.; Imanari, M.; Nicholson, L.; Cross, T. A. *Macromolecules* **1993**, *26*, 6660.
(26) Yoe, J. H.; Demura, M.; Asakura, T.; Fujito, Imanari, T.; Nicolson, M.; Cross, T. A. *Solid State NMR* **1994**, *3*, 209.
(27) Greenfield, M. S.; Ronemus, A. D.; Vold, R. L.; Vold, R. R.; Ellis, P. D.; Raidy, T. E. *J. Magn. Reson*. **1987**, *72*, 89.
(28) Seelig, J. Q. *Rev. Biophys. Acta* **1977**, *10*, 353.
(29) Davis, J. H. *Biochim. Biophys. Acta* **1983**, *117*, 737.
(30) Kinsey, R. A.; Kimtanar, A.; Isai, M.-D.; Smith, R. J.; James, N.; Oldfield, E. *J. Biol. Chem*. **1981**, *256*, 4146.
(31) Ulrich, A. S.; Watts, A.; Wallat, I.; Heyn, M. P. *Biochemistry* **1994**, *33*, 5370.
(32) Ulrich, A. S.; Watts, A. *Solid State NMR* **1993**, *2*, 21.
(33) Hentschel, R.; Sillescu, H.; Spiess, H. W. *Polymer* **1981**, *22*, 1516.
(34) Momany, F. A.; MacGuire, R. F.; Burgess, A. W.; Sheraga, H. A. *J. Phys. Chem*. **1975**, *79*, 2361.
(35) Asakura, T. *Makromol Chem*. **1981**, *182*, 1135.
(36) Shoemaker, D. P.; Barieau, R. E.; Donohue, J.; Lu, C. *Acta Crystallogr*. **1953**, *6*, 241.
(37) Frey, M. N.; Lehmann, M. S.; Koetzle, T. F.; Hamilton, W. *Acta Crystallogr*. **1973**, *B29*, 876.
(38) Kistenmacer, T. J.; Rand, G. A.; Marsh, R. E. *Acta Crystallogr*. **1974**, *B30*, 2573.
(39) Asakura, T.; Demura, M.; Watanabe, Y.; Sato, K. *J. Polym. Sci*. **1992**, *B30*, 693.
(40) Gary, T. M.; Matthews, B. W. *J. Mol. Biol*. **1984**, *175*, 75.
(41) Perczel, A.; Farkas, Ö.; Csizmadia, I. G. *J. Am. Chem. Soc*. **1996**, *118*, 7809.
(42) Demura, M.; Minami, M.; Asakura, T.; Cross, T. A. *J. Am. Chem. Soc*. **1998**, *120*, 1300.

MA990554Q